WISC

UC

UNIVERSITY OF WISCONSIN • MADISON, WISCONSIN

PLASMA PHYSICS

55
6-12-95
JS (2)

THE EFFECT OF COLLISIONALITY AND DIAMAGNETISM ON THE PLASMA DYNAMO

H. Ji[1], Y. Yagi[2], K. Hattori[2], A.F. Almagri[3], S.C. Prager[3], Y. Hirano[2], J.S. Sarff[3], T. Shimada[2], Y. Maejima[2], and K. Hayase[2]

DOE/ER/53198-259

May 1995

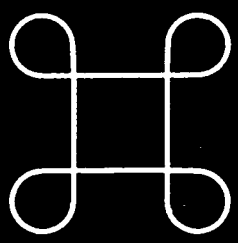

[illegible]

[illegible]

[illegible]

ONSIN

NOTICE

Printed in the United States of America
Available from
National Technical Information Service
U.S. Department of Commerce
5285 Port Royal Road
Springfield, VA 22161

NTIS Price codes
Printed copy: A02
Microfiche copy: A01

The Effect of Collisionality and Diamagnetism on the Plasma Dynamo

H. Ji[1], Y. Yagi[2], K. Hattori[2], A.F. Almagri[3], S.C. Prager[3],
Y. Hirano[2], J.S. Sarff[3], T. Shimada[2], Y. Maejima[2], and K. Hayase[2]

[1]*Plasma Physics Laboratory, Princeton University, P.O. Box 451, Princeton, New Jersy 08543*

[2]*Plasma Section, Electrotechnical Laboratory, Tsukuba, Ibaraki 305, Japan*

[3]*Department of Physics, University of Wisconsin, Madison, Wisconsin 53706*

(April 28, 1995)

Abstract

Fluctuation-induced dynamo forces are measured over a wide range of electron collisionality in the edge of TPE-1RM20 Reversed-Field Pinch (RFP). In the collisionless region the Magnetohydrodynamic (MHD) dynamo alone can sustain the parallel current, while in the collisional region a new dynamo mechanism resulting from the fluctuations in the electron diamagnetic drift becomes dominant. A comprehensive picture of the RFP dynamo emerges by combining with earlier results from MST and REPUTE RFPs.

PACS numbers: 52.55.Hc, 52.25.Gj, 52.35.Ra

The self-generation of a magnetic field (the dynamo) has been a long-standing mystery in astrophysical plasmas as well as in laboratory plasmas. The latter are the only examples in which the dynamo effect can be actively controlled and directly measured experimentally. In the reversed-field-pinch (RFP) plasma, the reversed toroidal field at the edge is generated and sustained by a poloidal dynamo force along the magnetic field line, which balances resistive dissipation. The most widely studied MHD dynamo model assumes that this parallel dynamo electric field arises from the correlation between the fluctuating flow velocity $\tilde{\boldsymbol{v}}$ and magnetic field $\widetilde{\boldsymbol{B}}$ [1], i.e., $< \tilde{\boldsymbol{v}} \times \widetilde{\boldsymbol{B}} >_{\parallel}$ where $< \ldots >$ denotes an average over an equilibrium flux surface. This model has been intensively employed in nonlinear computation [2], and agrees fairly well with experimental tearing mode spectra and their nonlinear mode interactions [3]. Alternatively, the kinetic dynamo theory (KDT) [4] is based on radial diffusion of the parallel current due to a prescribed stochastic magnetic field, consistent with the existence of a small population of fast electrons at the edge [5–7].

The first direct measurements of the MHD dynamo have been attempted in the REPUTE RFP edge [8]. The measured dynamo electric field was far below that required to balance resistive dissipation. On the other hand, recent measurements in the SPHEX spheromak [9] and MST RFP edge [10] have detected the MHD dynamo electric field to be of a direction and magnitude needed for the current sustainment. One of the most distinct differences between the two RFPs is that the MST edge is much more collisionless than REPUTE. Thus an important question still remains whether the MHD dynamo model is valid in general or limited to only certain conditions.

In this Letter, we report the results of dynamo measurements in the TPE-1RM20 RFP edge over a wide range of electron collisionality. The results confirm the existence of sufficient MHD dynamo electric field in the collisionless region. In the collisional case, however, the MHD dynamo diminishes while a new dynamo mechanism resulting from the electron pressure, i.e., the fluctuating electron diamagnetic drift, becomes dominant. This result encompasses the measurements in the REPUTE edge, leading to a more comprehensive picture of the dynamo phenomena over a wide range of the collisionality.

We write the parallel Ohm's law in a turbulent plasma, placing possible dynamo terms on the RHS [10],

$$\eta_{\|} j_{\|0} - E_{\|0} = < \tilde{v} \times \widetilde{B} >_{\|} - < \tilde{j} \times \widetilde{B} >_{\|} /en, \tag{1}$$

or alternatively by using $\tilde{v}_{\perp} - \tilde{j}_{\perp}/en \approx (\widetilde{E}_{\perp} \times B_0 + \nabla_{\perp} \tilde{P}_e \times B_0/en)/B^2$,

$$\eta_{\|} j_{\|0} - E_{\|0} = < \widetilde{E}_{\perp} \cdot \tilde{b}_{\perp} > + < \nabla_{\perp} \tilde{P}_e \cdot \tilde{b}_{\perp} > /en \tag{2}$$

where $b \equiv B/B$, η is the resistivity, j the current, E the electric field, P_e the electron pressure and n the electron density. The subscript 0 denotes the average values and the tilde denotes the fluctuations. Since $v \approx v_i$ and $j = en(v_i - v_e)$, Eq.(1) can be rewritten as

$$\eta_{\|} j_{\|0} - E_{\|0} = < (\tilde{v} - \tilde{j}/en) \times \widetilde{B} >_{\|} \approx < \tilde{v}_e \times \widetilde{B} >_{\|}, \tag{3}$$

where v_i (v_e) is the ion (electron) flow velocity. We note that the appearance of v_e only in the RHS is consistent with the parallel Ohm's law being a force balance of electrons.

The first term in the RHS of Eq.(2), $< \widetilde{E}_{\perp} \cdot \tilde{b}_{\perp} >$, represents the contribution to $\tilde{v}_{e\perp}$ from the fluctuating $\widetilde{E}_{\perp} \times B_0$ drift which is a MHD (single fluid) effect, while the second term, $< \nabla_{\perp} \tilde{P}_e \cdot \tilde{b}_{\perp} > /en$, is the contribution from the fluctuating electron diamagnetic drift $\nabla_{\perp} \tilde{P}_e \times B_0$ which is an electron fluid effect (in the two-fluid framework). Only the $E \times B$ effect has been incorporated in most MHD computations [2] where the *total* plasma pressure has usually been set to zero. The aim of the present experiments is to measure both the MHD dynamo term, $< \widetilde{E}_{\perp} \cdot \tilde{b}_{\perp} > \approx < \tilde{E}_t \tilde{b}_t > + < \tilde{E}_r \tilde{b}_r >$, and the electron diamagnetic term, $< \nabla_{\perp} \tilde{P}_e \cdot \tilde{b}_{\perp} > \approx < (\nabla_t \tilde{P}_e) \tilde{b}_t > + < (\nabla_r \tilde{P}_e) \tilde{b}_r >$ where the subscripts t and r denote the toroidal and radial components, respectively. Note the poloidal field B_p is much larger than the toroidal field B_t in the RFP edge.

The diagnostics used here are modified versions of those described in Ref. [10], including two versions of a complex probe [11] and a small, insertable Rogowskii coil probe [12] which measures the local poloidal (parallel) current. Each version of the complex probe consists of two triple probes to measure electron temperature T_e, density n, and floating potential V_f

at two locations separated by 1.27 cm toroidally (in the toroidal version) or 0.25 cm radially (in the radial version.) The toroidal version of the complex probe has been modified to block the fast electrons from the Tungsten tips with a small boron nitride obstacle while the radial version has been aligned so that the tips face away from fast electrons. Thus the fast electron effects on probe measurements are eliminated for the entire range of density.

The electrostatic components [13] of electric fields E_t and E_r are obtained from the difference in plasma potential $V_p = V_f + cT_e$, where $c \simeq 2.5$ (0.8) for E_t (E_r) calculated from the electron-ion collection area ratio at the different orientation of the probe tips with respect to the magnetic field [11]. Similarly, the fluctuations in gradient of the electron pressure are obtained from spatial differences. B_t and B_r and their fluctuations are measured by the magnetic pick-up coils installed in the complex probes.

The TPE-1RM20 [14] is a medium sized RFP device with major radius R of 0.75m, minor radius a of 0.192m, and plasma current up to 280kA. Field errors are minimized by a close-fitting triple shell structure [15] with the two thin shells at r=0.207m, 0.209m and the thick shell at r=0.215m. The experiments reported here were carried out at the relatively low plasma current I_p of $\simeq$ 50kA to avoid heat damage to the inserted probes. All measurements are taken around the current flattop period, typically during $t = 2 - 10$ ms. Each set of the measurements was carried out in 15-50 identical discharges, resulting in 400-2100 samples with a time interval of 0.2ms.

The collisionality scan is performed by changing the plasma density. In the normal operation for a fixed I_p, the line-averaged density $\bar{n}_e$ is primarily determined [16] by the pinch parameter Θ (defined by the ratio of $B_p(a)$ to the cross-section averaged B_t). For a given Θ, a higher filling pressure only results in a more drastic density "pump-out "during the start-up phase while maintaining the same density during the flattop phase. Typically, $\bar{n}_e$ ranges from $\simeq 0.44 \times 10^{19}/\mathrm{m}^3$ at $\Theta \simeq 1.5$ to $\simeq 1.01 \times 10^{19}/\mathrm{m}^3$ at $\Theta \simeq 2.0$. A higher density of $\bar{n}_e \simeq 1.86 \times 10^{19}/\mathrm{m}^3$ was achieved at the relatively high $\Theta \simeq 1.9$ by adding 15 wall loading discharges with D_2 gas before each main RFP discharge with the same working gas. (In contrast, the current MST operation [17] is limited to the relatively low density region

presumably due to its large size, R/a=1.50m/0.52m). By varying $\bar{n}_e$, the edge density at $r/a = 0.92$ increases by a factor of $\simeq 4$ while the electron temperature decreases by $\simeq 35\%$ (Fig. 1), yielding more than a factor of 10 change in the collisionality.

The cross correlation between two fluctuating quantities $\tilde{\alpha}$ and $\tilde{\beta}$ is given by

$$< \tilde{\alpha}\tilde{\beta} >= \int P_{\alpha\beta}(f)\mathrm{d}f = \int |\tilde{\alpha}(f)||\tilde{\beta}(f)|\gamma_{\alpha\beta}(f)\cos\theta_{\alpha\beta}(f)\mathrm{d}f,$$

where $P_{\alpha\beta}$ is the cross-power spectrum, $|\tilde{\alpha}|$ and $|\tilde{\beta}|$ are the fluctuation amplitudes, $\gamma_{\alpha\beta}$ and $\theta_{\alpha\beta}$ are coherence and relative phase between $\tilde{\alpha}$ and $\tilde{\beta}$, respectively. The Fast Fourier Transform method has been employed to calculate these quantities over each ensemble.

The cross-spectra of $< \widetilde{\boldsymbol{E}}_\perp \cdot \tilde{\boldsymbol{b}}_\perp >$ and $< \boldsymbol{\nabla}_\perp \tilde{P}_e \cdot \tilde{\boldsymbol{b}}_\perp > /en$ are shown in Fig.2(a) for four different densities. For both cross-spectra, the dominant frequency decreases with increased density, implying a decline in the plasma rotation velocity and/or in the real frequency. On the other hand, the MHD dynamo term (the solid curves) dominates over the electron diamagnetic term (the dotted curves) for the three relatively low density cases while the latter becomes larger for the highest density case. This relative variation arises mainly from changes in the coherence (shown in Fig.2(b)) as well as in the fluctuation levels (not shown). The coherence is comparable at the low density cases. When the density increases, however, coherence in the MHD dynamo term decreases nearly to the statistical confidence level determined by the number of samples in the ensemble ($1/\sqrt{N}$). On the other hand, coherence in the electron diamagnetic term remains roughly constant. The relative phase angle is ~ 0 (in phase) for all cases and changes little with density.

To establish the strength of the fluctuation-induced dynamo forces, in Fig.3 we compare them to the resistive term ηj where η is Spitzer's resistivity calculated from the measured local T_e but estimated $Z_{\mathrm{eff}} = 2$. Note $E_\parallel \approx E_p = 0$ in the steady state. For the three relatively low density cases, the MHD dynamo alone is sufficient to account for the resistive term, confirming the MHD dynamo hypothesis. However, in the highest density case the MHD dynamo diminishes while the electron diamagnetic term becomes dominant. The sum of the two terms is large enough to account for the ηj term within error bars. Contribution

of the fast electrons to the electron diamagnetic term, i.e., $< \nabla_\perp \tilde{P}_e^{\rm fast} \cdot \tilde{b}_\perp > /en$, is expected to be insignificant since the fast electron density is only a few percent of the bulk density [7].

The observation in TPE unites the earlier, apparently contradictory measurements in REPUTE and MST [10]. Figure 4(a) displays the cross-spectra and coherences of the dynamo forces measured in the MST edge. The samples are taken from 36 identical discharges with $I_p \simeq 130$kA and $\bar{n}_e \simeq 6.2 \times 10^{18}/\mathrm{m}^3$. As in the low density case of TPE, the MHD dynamo term dominates over the electron diamagnetic term. (The coherences at the high frequency region have a quite difference behavior than in TPE plasma but no contributions to the dynamo field.) On the other hand, no coherent MHD dynamo is detected in the high density REPUTE plasmas ($I_p \simeq 110$kA and $\bar{n}_e \simeq 4.4 \times 10^{19}/\mathrm{m}^3$), as shown in Fig.4(b), consistent with the TPE observations. The electron diamagnetic term has not been measured in REPUTE.

Thus a systematic dependence of the dynamo forces on the collisionality emerges from all three RFPs. A summary is given in Fig.5 where the dynamo forces and their resistive terms (normalized by $E_0 = V_{\rm loop}/2\pi R$) are plotted against the electron mean free path (normalized by the plasma radius a) which is varied by more than a factor of 30. Clearly, in the collisionless region ($\lambda_e/a \gtrsim 1$), the MHD dynamo is the main driver of the parallel current, while in the collisional region ($\lambda_e/a \lesssim 1$), the electron diamagnetic dynamo term becomes dominant. Following this categorization, the ZETA plasma [18] falls into the collisional region while other RFP plasmas, such as ZT-40M [19], fall into the collisionless region where the MHD dynamo should dominate, as marked in Fig.5. The observation implies the ineffectiveness of the KDT mechanism [4] which is expected to be activated in the collisionless region. On the other hand, the observation is consistent with the Terry-Diamond theory [20] which incorporates self-consistent constraints and predicts negligible kinetic dynamo effect in the collisionless limit.

We can interpret the results via either Eq.(1) or Eq.(2). At low collisionality, the MHD

dynamo dominates. Hence the $< \tilde{\boldsymbol{v}} \times \widetilde{\boldsymbol{B}} >$ term is large in Eq.(1). The cross-field flow $\tilde{\boldsymbol{v}}_\perp$ establishes an electric field $\widetilde{\boldsymbol{E}}_\perp$ self-consistently through charge separation. As a result, the dynamo field $\tilde{\boldsymbol{v}}_\perp \times \widetilde{\boldsymbol{B}}_\perp = \widetilde{\boldsymbol{E}}_\perp \cdot \widetilde{\boldsymbol{B}}_\perp / B_0$ is large in Eq.(2). Both electrons and ions move together and the Hall term [21] in Eq.(1) is small, consistent with MST measurements [22].

At high collisionality, the electron pressure term in Eq.(2) is large. Fluctuations in the electron pressure gradient (instead of the electric field) sustain the fluctuating electron flow velocity self-consistently. This effect would be manifest in Eq.(1) as a Hall dynamo arising from the fluctuating electron diamagnetic current $\tilde{\boldsymbol{j}}_{e\perp} = \boldsymbol{B}_0 \times \boldsymbol{\nabla} \tilde{P}_e / B_0^2$. The ion flow is unspecified. If one assumes strong coupling between electrons and ions, i.e., $\tilde{P}_e \approx \tilde{P}_i$, as likely in the collisional limit, then the ion diamagnetic drift $\tilde{\boldsymbol{v}}_{i\perp} (= -\boldsymbol{\nabla}_\perp \tilde{P}_i \times \boldsymbol{B}_0 / enB_0^2)$ is opposite to the electron diamagnetic drift, resulting in an anti-dynamo effect in the $\tilde{\boldsymbol{v}} \times \widetilde{\boldsymbol{B}} \approx \tilde{\boldsymbol{v}}_i \times \widetilde{\boldsymbol{B}}$ term in Eq.(1). However, this is offset by an additional dynamo effect in the Hall term from the associated ion diamagnetic current $\tilde{\boldsymbol{j}}_{i\perp} = \boldsymbol{B}_0 \times \boldsymbol{\nabla} \tilde{P}_i / B_0^2$.

We suggest two possible physical reasons for the transition by collisions. First, an increase in the perpendicular conductivity with collisions can suppress the electric field. Second, the collisions could reduce $\tilde{\boldsymbol{v}}_{i\perp}$ through the ion perpendicular viscosity $\nu_{i\perp} \propto n^2 / \sqrt{T_i}$ [23]. The differential perpendicular electron and ion flows result in a perpendicular current $\tilde{\boldsymbol{j}}_\perp$ which establishes the pressure gradient by $\tilde{\boldsymbol{j}}_\perp \times \boldsymbol{B}_0$ force in a self-consistent way. In any case, as implied by Eq.(3), the dynamo is carried out by electron dynamics only, consistent with the fact that the generated reversed toroidal field component is indeed produced by the fast-moving electrons.

In conclusion, we have identified a new dynamo effect arising from electron diamagnetism. In the collisionless region, the MHD dynamo alone can sustain the parallel current, confirming the earlier results from MST. On the other hand, the new electron diamagnetic dynamo term becomes dominant in the collisional region, recovering the REPUTE results. These observations resolve the discrepancy from earlier results, suggesting a comprehensive picture of the dynamo phenomena over a wide range of the collisionality. Since existing and

future RFPs are operated mostly in the collisionless region, the observations suggest that the MHD picture of the RFP dynamo should be prevalent. The common observation of an increasing fast electron population with decreasing density can be consistent with the MHD dynamo: the electrons are more easily accelerated to high energy in less collisional plasmas, for a given dynamo force.

On of the authors (H.J.) is grateful to Dr. M. Yamada and C. Sovinec for valuable discussions. This work was supported by the U.S. Department of Energy and Japanese Science and Technology Agency.

REFERENCES

[1] H.K. Moffatt, in *Magnetic Field Generation in Electrically Conducting Fluids* (Cambridge University Press, 1978)

[2] For example, an early simulation result is E.J. Caramana, R.A. Nebel and D.D. Schnack, Phys. Fluids, **26**, 1305(1983); and a recent one is A. Nagata, H. Sakamoto, K. Sato, H. Ashida, T. Amano, Phys. Plasmas, **2**, 1182(1995).

[3] S. Assadi, S.C. Prager, and K.L. Sidikman, Phys. Rev. Lett. **69**, 281(1992).

[4] A.R. Jacobson and R.W. Moses, Phys. Rev. A, **29**, 3335(1984).

[5] J.C. Ingraham, R.F. Ellis, J.N. Downing, C.P. Munson, P.G. Weber, and G.A. Wurden, Phys. Fluids, **B2**, 143(1990).

[6] M.R. Stoneking, S.A. Hokin, S.C. Prager, G. Fiksel, H. Ji, and D.J. Den Hartog, Phys. Rev. Lett. **73**, 549(1994).

[7] Y. Yagi, Y. Hirano, Y. Maejima, P.R. Brunsell, T. Shimada, and K. Hattori, ETL Technical Report, No. TR-93-22(1993).

[8] H. Ji, H. Toyama, A. Fujisawa, S. Shinohara, and K. Miyamoto, Phys. Rev. Lett. **69**, 616(1992).

[9] A. al-Karkhy, P.K. Browning, G. Cunningham, S.J. Gee, and M.G. Rusbridge, Phys. Rev. Lett. **70**, 1814(1993).

[10] H. Ji, A.F. Almagri, S.C. Prager, and J.S. Sarff, Phys. Rev. Lett. **73**, 668(1994).

[11] H. Ji, H. Toyama, K. Yamagishi, S. Shinohara, A. Fujisawa, and K. Miyamoto, Rev. Sci. Instrum., **62**, 2326(1991).

[12] A.F. Almagri, S. Assadi, S.C. Prager, J.S. Sarff, and D.W. Kerst, Phys. Fluids, **B4**, 4080(1992).

[13] The inductive components are negligible.

[14] Y. Yagi *et al.*, in *Plasma Phys. and Controlled Nuclear Fusion Research 1992* (International Atomic Energy Agency, Vienna, 1993), **2**, 661(1993).

[15] Y. Yagi *et al.*, J. Plasma Fusion Res., **69**, 700(1993).

[16] Y. Yagi, P.R. Brunsell, Y. Hirano, I. Hirota, Y. Maejima, and T. Shimada, in *Plasma Phys. and Controlled Nuclear Fusion Research 1994* (International Atomic Energy Agency, Vienna, 1995), paper No. C-1-I-3. (to be published)

[17] R.N. Dexter, D.W. Kerst, T.W. Lovell, S.C. Prager, and J.C. Sprott, Fusion Technol. **19**, 131(1991).

[18] M.G. Rusbridge, Plasma Phys., **11**, 35(1969).

[19] H.Y.W. Tsui *et al.*, Nucl. Fusion, **31**, 2371(1991).

[20] P.W. Terry and P.H. Diamond, Phys. Fluids, **B2**, 1128(1990).

[21] L. Turner, IEEE Trans. Plasma Science, **PS-14**, 849(1986).

[22] W. Shen and S.C. Prager, Phys. Fluids, **B7**, 1931(1993).

[23] S.I. Braginskii, in *Reviews of Plasma Physics* (Consultants Bureau, New York, 1965), **1**, p.205.

FIGURES

FIG. 1. Edge density and electron temperature in TPE-1RM20 measured at $r/a = 0.92$ in the scan of the line-averaged density.

FIG. 2. Cross spectra (a) and coherence (b) for the MHD dynamo term and the electron diamagnetic dynamo term for the four different density cases in TPE-1RM20.

FIG. 3. Comparison of the dynamo terms to the resistive term ηj as a function of the local density in TPE-1RM20.

FIG. 4. Cross spectra and coherence of the dynamo forces measured in MST (a) and REPUTE (b).

FIG. 5. Normalized dynamo terms and resistive term ηj versus normalized electron mean free path in the edge of TPE, MST and REPUTE plasmas. Also shown is the collisionality ranges for the ZETA and ZT-40M edge.

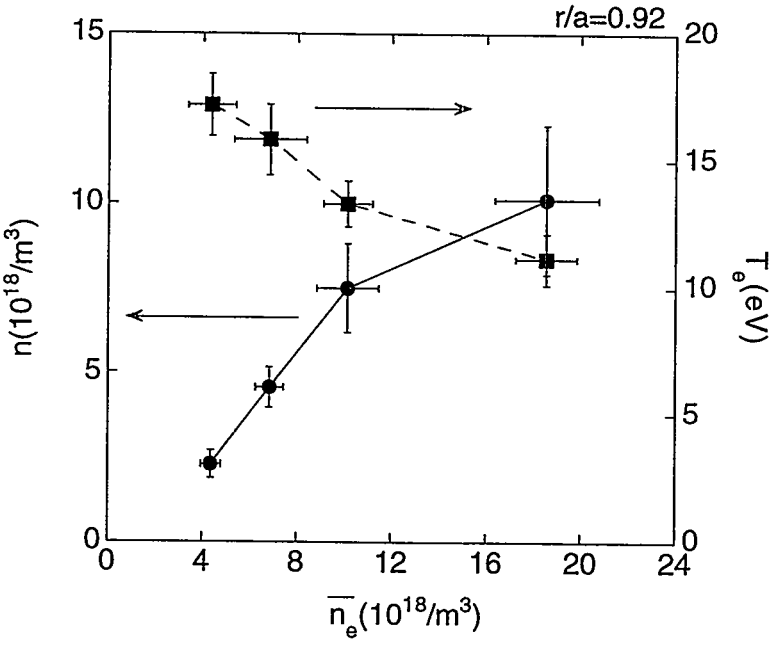

Figure 1

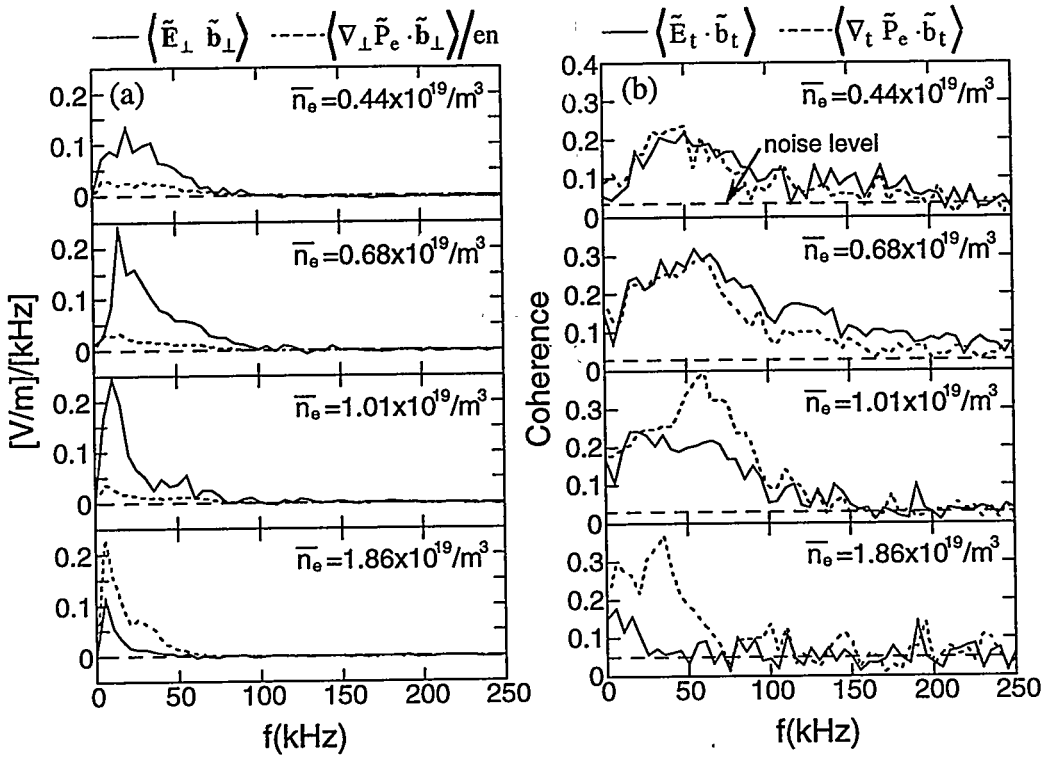
(a)
(b)
$\overline{n_e}$=0.44x10^{19}/m^3
$\overline{n_e}$=0.68x10^{19}/m^3
$\overline{n_e}$=1.01x10^{19}/m^3
$\overline{n_e}$=1.86x10^{19}/m^3
noise level
[V/m]/[kHz]
Coherence
f(kHz)
f(kHz)

Figure 2

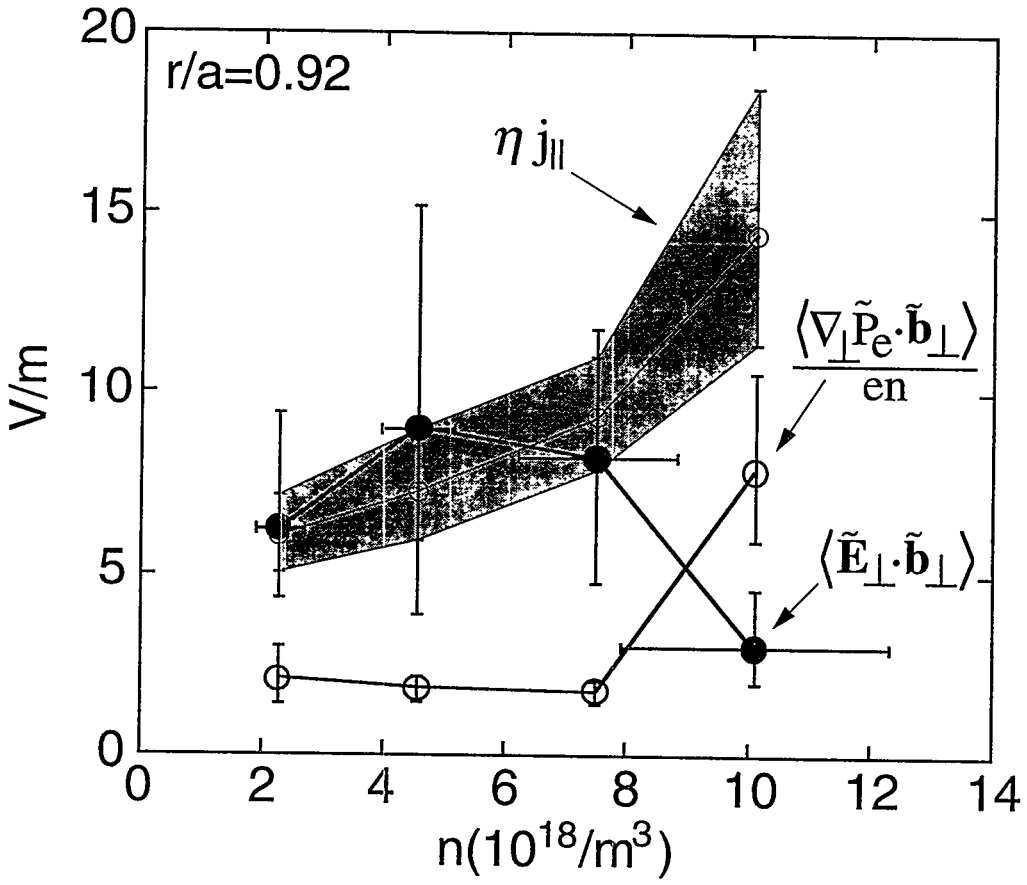
r/a=0.92
$\eta\, j_{\|}$
$\frac{\langle \nabla_\perp \tilde{P}_e \cdot \tilde{b}_\perp \rangle}{en}$
$\langle \tilde{E}_\perp \cdot \tilde{b}_\perp \rangle$
V/m
$n(10^{18}/m^3)$
0
5
10
15
20
0
2
4
6
8
10
12
14

Figure 3

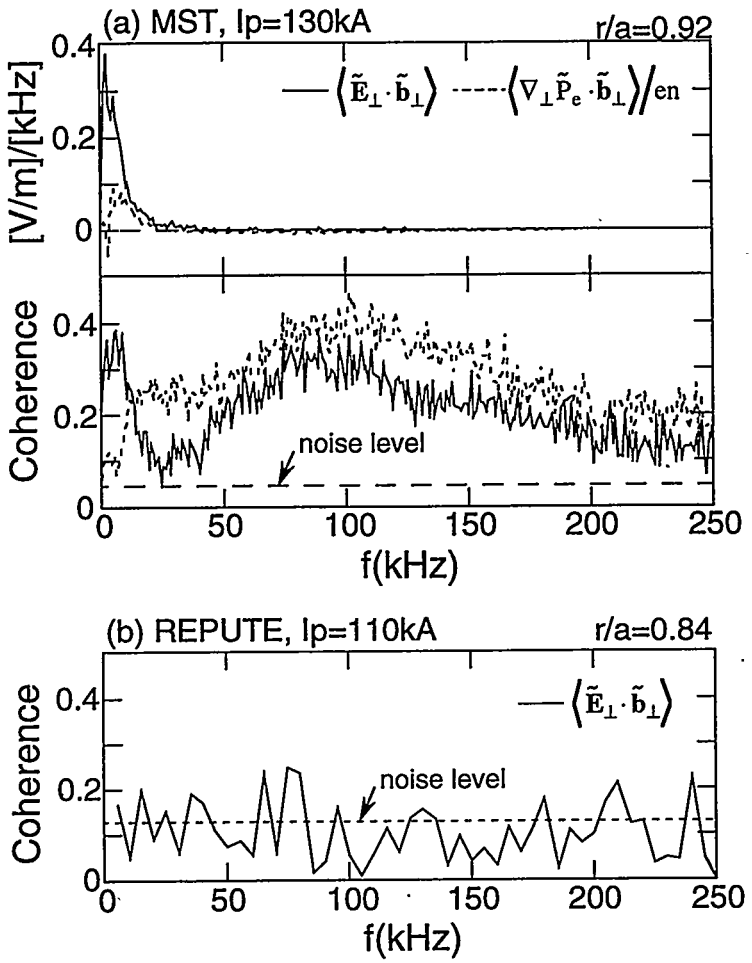
(a) MST, Ip=130kA
r/a=0.92
$\langle \tilde{E}_\perp \cdot \tilde{b}_\perp \rangle$
$\langle \nabla_\perp \tilde{P}_e \cdot \tilde{b}_\perp \rangle / en$
[V/m]/[kHz]
Coherence
noise level
f(kHz)
(b) REPUTE, Ip=110kA
r/a=0.84
$\langle \tilde{E}_\perp \cdot \tilde{b}_\perp \rangle$
noise level
Coherence
f(kHz)

Figure 4

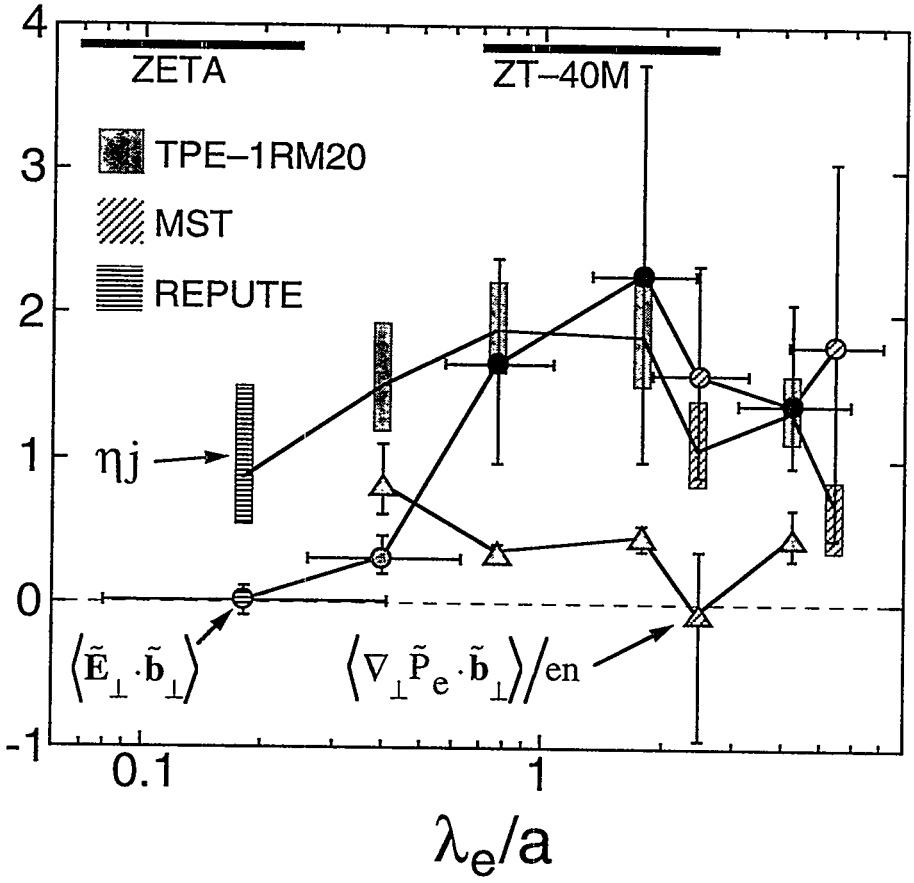
ZETA
ZT–40M
TPE–1RM20
MST
REPUTE
ηj
$\langle \tilde{\mathbf{E}}_\perp \cdot \tilde{\mathbf{b}}_\perp \rangle$
$\langle \nabla_\perp \tilde{P}_e \cdot \tilde{\mathbf{b}}_\perp \rangle / en$
4
3
2
1
0
-1
0.1
1
λ_e/a

Figure 5

EXTERNAL DISTRIBUTION IN ADDITION TO UC-20

S.N. Rasband, Brigham Young University
T. Dolan, EG&G Idaho, Inc.
R.A. Moyer, General Atomics
J.B. Taylor, Institute for Fusion Studies, The University of Texas at Austin
E. Uchimoto, University of Montana
F.W. Perkins, PPPL
O. Ishihara, Texas Technical University
M.A. Abdou, University of California, Los Angeles
R.W. Conn, University of California, Los Angeles
P.E. Vandenplas, Association Euratom-Etat Belge, Belgium
Centro Brasileiro de Pesquisas Firicas, Brazil
P. Sakanaka, Institute de Fisica-Unicamp, Brazil
Mme. Monique Bex, GANIL, France
J. Radet, CEN/CADARACHE, France
University of Ioannina, Greece
R. Andreani, Associazione EURATOM-ENEA sulla Fusione, Italy
Biblioteca, Istituto Gas Ionizzati, EURATON-ENEA-CNR Association, Italy
Plasma section, Energy Fundamentals Division Electrotechnical Laboratory, Japan
Y. Kondoh, Gunma University, Kiryu, Gunma, Japan
H. Toyama, University of Tokyo, Japan
Z. Yoshida. University of Tokyo, Japan
FOM-Instituut voor Plasmafysica "Rijnhuizen," The Netherlands
Z. Ning, Academia Sinica, Peoples Republic of China
P. Yang, Shandong University, Peoples Republic of China
S. Zhu, University of Science & Technology of China, People's Republic of China
I.N. Bogatu, Institute of Atomic Physics, Romania
M.J. Alport, University of Natal, Durban, South Africa
R. Storer, The Flinders University of South Australia, South Australia
B. Lehnert, Royal Institute of Technology, Sweden
Librarian, CRPP, Ecole Polytechnique Federale de Lausanne, Switzerland
B. Alper, Culham Laboratory, UK
A. Newton, UK

2 for Chicago Operations Office
5 for individuals in Washington Offices

INTERNAL DISTRIBUTION IN ADDITION TO UC-20
80 for local group and file